RESEARCH PAPER

Execution of Artificial Intelligence Algorithms in the Dilution Analysis of Super Duplex Stainless Steel Clads

Kalpna suman, Mohd Majid*, Nidhi Yaduvanshi, Sachin Pachauri, Gaurav Verma*, Abhinav Saxena

Department of computer science and engineering, LDAH Rajkiya Engineering College Mainpuri, Uttar pradesh, India, Email: kalpnasuman.jsu@gmail.com
Department of Mechanical Engineering, Sant Longowal Institute of Engineering and Technology, Longowal, Punjab, India, Email: mohdmajid@sliet.ac.in
Department of Physics, JSS University Noida, Uttar pradesh, India, Email: nidhi.yaduvanshi@jssuninoida.edu.in
Department of Electrical Engineering LDAH Rajkiya Engineering College Mainpuri, Uttar pradesh, India, Email: sachinpachauri@recmainpuri.in
Department of Electrical Engineering LDAH Rajkiya Engineering College Mainpuri, Uttar pradesh, India, Email: gaurav.verma@recmainpuri.in
Department of Electrical Engineering, J. C. Bose University of Science and Technology, YMCA, Faridabad, Haryana, Email: abhinaviitroorkee@gmail.com
***Corresponding Author**
Email: mohdmajid@sliet.ac.in, gaurav.verma@recmainpuri.in
Received:1st September,2026; **Revised:**5th September,2026; **Accepted:**8th September,2026; **Available Online:**20th September, 2026

Abstract
A comprehensive, repeatable machine-learning approach for anticipating and managing the dilution of super duplex stainless steel (SDSS) weld claddings deposited on carbon steel is shown in this research. The bead cross-section is used to formalize dilution geometrically, and a mixing rule that extends to the Creq/Nieq ratio and the pitting resistance equivalent number (PREN) is used chemically. Five process inputs—current, voltage, travel speed, wire feed rate, and contact-tip-to-work distance—are used to train five regressors: ridge regression, support vector regression, random forest, gradient boosting, and a multilayer perceptron.Inverse optimization is then carried out using a real-coded genetic algorithm, which maximizes wire feed rate within a dilution limit. The dataset (n = 360) is produced using a physics-informed bead-formation model with measurement-scale noise rather than from laboratory experiments because this work is a methodological demonstration. Support vector regression produced the best overall result on the held-out set ($R^2 = 0.930$, RMSE = 1.01 percentage points; five-fold cross-validated $R^2 = 0.945$). In accordance with the process model (7.2%), the evolutionary algorithm converged to a parameter set with an anticipated dilution of 7.3%. Data from spectrometry and measured macrographs can be used directly with the pipeline, which is data-agnostic.
Index Terms—super duplex stainless steel, weld cladding, dilution, machine learning, support vector regression, genetic algorithm, PREN.

How to cite this article: Suman K, Majid M, Yaduvanshi N, Pachauri S, Verma G, Saxena A., Execution of Artificial Intelligence Algorithms in the Dilution Analysis of Super Duplex Stainless Steel Clads. Int J Drug Deliv Technol. 2026;16(90s): 470-478; DOI: 10.25258/ijddt.16.90s.45

I.Introduction

About 25 weight percent Cr, 7–9 weight percent Ni, 3–4 weight percent Mo, and 0.24–0.32 weight percent N are found in super duplex stainless steels (SDSS). Excellent resistance to pitting, crevice corrosion, and chloride stress corrosion cracking is provided by their nearly equal mix of ferrite and austenite, which combines high strength with a PREN above 40 [1]–[3]. For pressure vessels, subsea equipment, and chemical process plants, a thin coating of SDSS is often formed via arc weld overlay (cladding) on carbon or low-alloy steel due to the high cost of bulk SDSS [1].

Dilution, or the portion of the deposit that comes from melting substrate, is the crucial metallurgical quantity in cladding. Iron-rich dilution reduces the deposit's Cr, Mo, and N content, which lowers PREN and shifts the Creq/Nieq balance away from the desired ferrite–austenite ratio [1], [5], and [6]. The process window is confined on both sides because too little dilution could result in a lack of fusion. Heat input, deposition rate, and torch shape all interact nonlinearly to determine dilution [6], [7].Response-surface regression is

typically used to model dilution on planned experiments [6], [7]. More adaptable nonlinear mappings are provided by artificial intelligence (AI) techniques like neural networks [8], and process parameters can be chosen by inverting the learned model using metaheuristics like genetic algorithms (GA) [12]. These components are combined in this study into a single procedure that is connected to SDSS acceptance criteria. The contributions include: (i) a mathematical framework that connects geometric dilution, chemical mixing, PREN, and Creq/Nieq; (ii) five regression algorithms are implemented and compared; (iii) GA-based inverse optimization under dilution and process-coupling constraints; and (iv) permutation-based explainability of the trained model.

Pressure vessels, subsea manifolds, heat exchangers, valve bodies, and piping used in oil and gas, desalination, and chemical processing are all frequently covered with corrosion-resistant alloy (CRA) overlays. It is more cost-effective to deposit a corrosion-resistant layer on a low-cost carbon or low-alloy steel substrate than to make components wholly of CRA. Because of their roughly balanced ferritic–austenitic microstructure, which combines high strength with PREN values surpassing 40, super duplex stainless steels, which contain approximately 25% Cr, 7–9% Ni, 3–4% Mo, and 0.25–0.30% N, are especially well adapted to sour and chloride-rich environments [15], 16.

The deposited metal in weld cladding invariably blends with the molten base metal. This mixture, known as dilution, lowers the concentration of alloying components while adding iron to clad. During multi-pass deposition or post-weld heat treatment, even little over-dilution for SDSS overlays can lower Cr, Mo, and N levels sufficiently to drive the PREN below specification, destabilize the phase balance toward ferrite, and encourage secondary phases like sigma and chi [15], [17]. Low dilution increases the likelihood of inadequate metallurgical bonding and absence of fusion. Therefore, industry practice focuses on a small dilution window, typically 5–15%, that strikes a compromise between chemical performance and bond integrity. Heat input, arc force, wire melting rate, bead geometry, shielding gas, and joint geometry all interact intricately and nonlinearly to control dilution. Previous research used factorial design and multiple regression to establish empirical connections between process factors and bead geometry or dilution in surfacing procedures [18], [19]. Polynomial regression models are useful, but they degrade away from the design points, assume a fixed functional form, and perform badly when parameter space is large. Although they provide insight, physics-based thermal models, such those based on the double-ellipsoidal heat source [20], are computationally costly and need to be calibrated for every combination of materials and processes.

A data-driven substitute is provided by artificial intelligence. While ensemble tree approaches capture threshold effects and interactions without explicit specification [22], [23], neural networks are universal function approximators [21]. These models can search the parameter space much more quickly than physical trials when combined with evolutionary optimizers [24], [25]. Nevertheless, published research on AI-assisted dilution analysis typically focuses only on bead geometry, seldom links geometry to chemical results (Cr, Mo, N, PREN, ferrite number), and frequently ignores model interpretability, which restricts welding engineers' adoption.

II. Dilution and Metallurgical mathrmatical model

A. Heat Input and Geometric Dilution

For a single-pass bead, the arc heat input is

$$HI = \frac{\eta U I}{1000 v} \tag{1}$$

where U is arc voltage (V), I is current (A), v is travel speed (mm/s), $\eta = 0.8$ is the assumed arc efficiency and HI is in kJ/mm. If the filler wire of diameter d_w is fully deposited, mass conservation gives the reinforcement area

$$A = \frac{(1000\,\mathrm{WFS}/60)\,\pi d_w^2/4}{v} \tag{2}$$

with wire feed rate WFS in m/min. Let B be the cross-sectional area of melted substrate and A the area of the clad above the original surface (Fig. 1). The geometric dilution is

$$D = \frac{B}{A+B} \times 100\,\% \tag{3}$$

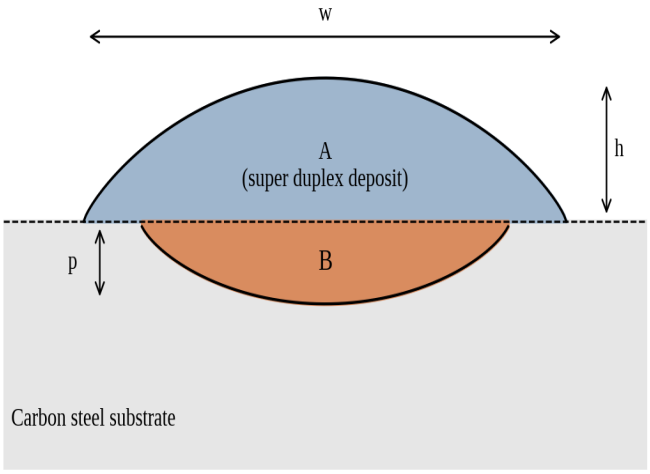

Fig. 1. Cross-section of a single clad bead. A: reinforcement (filler) area, B: melted base-metal area, h: reinforcement height, p: penetration, w: bead width.

Equation (3) shows why dilution falls when WFS rises (larger A) and rises with heat input (larger B).

B. Chemical Dilution, PREN and Multilayer Cladding

Under ideal homogeneous mixing, the chemical dilution computed from the Cr content of filler (f), deposit (d) and base (b) is

$$D_c = \frac{w_{\mathrm{Cr}}^{f} - w_{\mathrm{Cr}}^{d}}{w_{\mathrm{Cr}}^{f} - w_{\mathrm{Cr}}^{b}} \tag{4}$$

and the deposit composition of any element i follows the mixing rule

$$w_i^{d} = (1 - D)\, w_i^{f} + D\, w_i^{b} \tag{5}$$

so that $D_c \approx D$ when mixing is complete. The pitting resistance equivalent number is [4]

$$\mathrm{PREN} = w_{\mathrm{Cr}} + 3.3\, w_{\mathrm{Mo}} + 16\, w_{\mathrm{N}} \tag{6}$$

with contents expressed in weight percent. The carbon steel has PREN ≈ 0.2 and the filler has PREN = 41.9 for the typical compositions in Table I. Thus, PREN = 37.7, below 40, for a single layer at D = 10%. For this reason, SDSS overlays are typically applied in two or more layers. As each subsequent layer is diluted by the preceding deposit, the n-th layer has

$$\mathrm{PREN}_n = (1 - D)\,\mathrm{PREN}^{f} + D\,\mathrm{PREN}_{n-1} \tag{7}$$

which for D = 10 % gives $\mathrm{PREN}_2 = 41.5$ (≥ 40). The analysis shows that a first-layer limit near D ≈ 10 % is compatible with a corrosion-resistant top layer.

TABLE I
REPRESENTATIVE COMPOSITIONS USED (WT%)

Element	Carbon steel (base)	SDSS filler
C	0.15	0.02
Cr	0.10	25.0
Ni	0.05	9.5
Mo	0.00	3.9
N	0.005	0.25
Cu	0.10	0.30
PREN	0.2	41.9

C. Phase Balance

Using the WRC-1992 equivalents [5], the chromium and nickel equivalents are

$$\mathrm{Cr}_{eq} = w_{\mathrm{Cr}} + w_{\mathrm{Mo}} + 0.7\, w_{\mathrm{Nb}} \tag{8}$$

$$\mathrm{Ni}_{eq} = w_{\mathrm{Ni}} + 35\, w_{\mathrm{C}} + 20\, w_{\mathrm{N}} + 0.25\, w_{\mathrm{Cu}} \tag{9}$$

The Creq/Nieq ratio decreases from 1.89 for undiluted filler to 1.82 at D = 10% (Fig. 2) when Eqs. (5), (8), and (9) are applied to Table I. This is because carbon from the substrate increases Nieq while Cr and Mo are diluted. This is not a ferrite-number prediction; rather, it is an example of mixing rules.

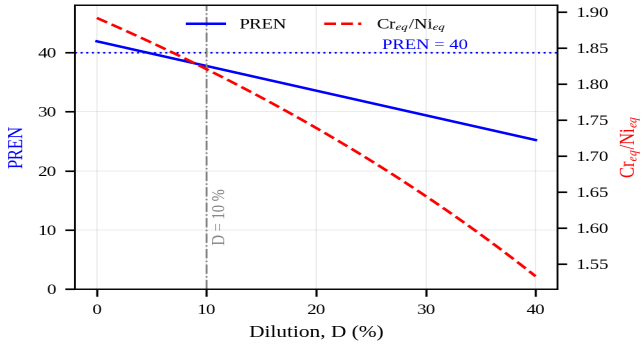

Fig. 2. Effect of dilution on PREN (left axis) and Cr_{eq}/Ni_{eq} (right axis) from the mixing rule and Table I compositions.

III. METHODOLOGY

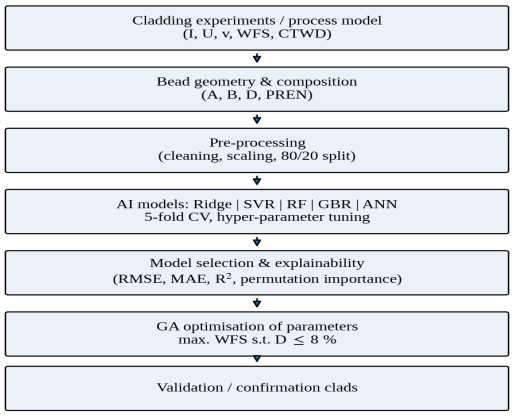

Fig. 3. Workflow of the proposed AI-based dilution analysis and optimisation.

A. Dataset

A total of 288 training and 72 test samples (80/20 split of n = 360) were produced. The five variables in Table II are the inputs, and like in synchronous gas metal arc processes, WFS is connected with current. From Eqs. (1)–(3), A and B were calculated using

$$B = 7.0\,HI^{1.9} f_c f_w \tag{10}$$

where fw = 1 − 0.30 tanh((WFS − 8)/2.5) and fc = 1 + 0.03(CTWD − 17). Measurement scatter is simulated with log-normal noise (σ = 0.07 on B, 0.03 on A). The coefficients were not calibrated to any particular experiment; they are merely illustrative. Therefore, rather than being experimental findings, the results are a demonstration of the process. In reality, image analysis would be used to measure A and B from etched macrographs, and spectrometry would use Eq. (4) to cross-check the results.

TABLE II
PROCESS VARIABLES AND GENERATED DATA

Quantity	**Range / value**
Current I (A)	120–260
Voltage U (V)	18–30
Travel speed v (mm/s)	3–10
Wire feed rate WFS (m/min)	≈ 0.04I ± 0.5 (4–12)
CTWD (mm)	12–22
Wire diameter, η	1.2 mm, 0.8
Heat input (kJ/mm)	0.22–1.66
Dilution D (%)	3.7–25.5 (mean 10.6, SD 4.1)

B. AI Algorithms

All inputs are standardised using the training-set mean and standard deviation:

$$\mathbf{z} = (\mathbf{x} - \boldsymbol{\mu}) \oslash \boldsymbol{\sigma} \tag{11}$$

The artificial neural network (ANN) is a 5–12–6–1 perceptron with tanh activations [9]:

$$\hat{D} = \mathbf{w}_3^{\top} \tanh(\mathbf{W}_2 \tanh(\mathbf{W}_1 \mathbf{z} + \mathbf{b}_1) + \mathbf{b}_2) + b_3 \tag{12}$$

It is trained by minimising the regularised mean-squared error

$$\mathcal{L} = \frac{1}{n} \sum_{k=1}^{n} (D_k - \hat{D}_k)^2 + \lambda \sum_{l} \|\mathbf{W}_l\|_F^2 \tag{13}$$

with the L-BFGS optimiser. Support vector regression (SVR) with a radial basis kernel [14] predicts

$$\hat{D}(\mathbf{x}) = \sum_{k} (\alpha_k - \alpha_k^*) e^{-\gamma \|\mathbf{x} - \mathbf{x}_k\|^2} + b \tag{14}$$

where α_k and α_k^* are dual coefficients. Random forest (RF) [10] averages T decision trees h_t:

$$\hat{D}_{RF}(\mathbf{x}) = \frac{1}{T} \sum_{t=1}^{T} h_t(\mathbf{x}) \tag{15}$$

Gradient boosting regression (GBR) [11] builds an additive model stage by stage:

$$F_m(\mathbf{x}) = F_{m-1}(\mathbf{x}) + \nu \gamma_m h_m(\mathbf{x}) \tag{16}$$

where ν is the learning rate. Ridge regression, a linear model with L2 penalty, serves as the baseline. All models were implemented in scikit-learn [13]. Hyper-parameters (Table III) were set from a small manual search using five-fold cross-validation on the training set only.

C. Evaluation and Explainability

Accuracy is assessed on the held-out set by

$$\mathrm{RMSE} = \sqrt{\frac{1}{n} \sum_{k=1}^{n} (D_k - \hat{D}_k)^2} \tag{17}$$

$$R^2 = 1 - \frac{\sum_{k} (D_k - \hat{D}_k)^2}{\sum_{k} (D_k - \bar{D})^2} \tag{18}$$

and by the mean absolute error (MAE). The influence of input j is quantified by permutation importance [10],

$$\mathrm{PI}_j = \mathrm{RMSE}(\mathbf{X}^{(j,\pi)}) - \mathrm{RMSE}(\mathbf{X}) \tag{19}$$

where $X^{(j,\pi)}$ denotes the test matrix with column j randomly shuffled (50 repetitions).

D. Genetic-Algorithm Optimisation

The trained best model is inverted by a real-coded GA [12] that maximises productivity (WFS) subject to a dilution limit D_{max} = 8 % and to a coupling constraint that keeps WFS near the range supported by the training data:

$$\max_{\mathbf{x}} f(\mathbf{x}) = \mathrm{WFS} - P(\mathbf{x}) \tag{20}$$

$$P = \kappa \left[\max(0, \hat{D} - D_{max}) + \max(0, |\mathrm{WFS} - 0.04I| - 1) \right] \tag{21}$$

with κ = 5. The GA uses a population of 60, 60 generations, tournament selection (size 3), elitism, Gaussian mutation (probability 0.15, σ = 0.1 of the variable range) and blend crossover (probability 0.85),

$$\mathbf{x}' = \mathrm{clip}(a\,\mathbf{x}_1 + (1-a)\,\mathbf{x}_2,\ \mathbf{x}_{lb}, \mathbf{x}_{ub}) \tag{22}$$

where a ~ U(0, 1). Five independent runs were performed and the best was retained.

E) Artificial Neural Network**.** The Adam optimizer [14] with mean squared error loss, L2 weight regularization, and early stopping on the validation loss was used to train a fully connected feed-forward network with an input layer of nine features, two hidden layers (e.g., 16 and 8 neurons) with ReLU or tanh activation, and an output layer of four neurons. Bayesian or random search was used to adjust the hyperparameters (layer widths, learning rate, and regularization strength).

F) Support Vector Regression**.** For every response, an ε-insensitive SVR with a radial basis function kernel [15] was trained separately, using grid search to adjust C, ε, and γ.

G) Random Forest**.** An ensemble of decision trees trained on bootstrap samples with random feature subsets at each split [8], tuning the number of trees, maximum depth and minimum leaf size.

IV. Results and Discussion

A. Predictive Accuracy

The five models are compared in Table III and Fig. 4. Ridge regression and SVR are tied on test RMSE (1.01 and 1.01 percentage points), but SVR was chosen because it had a lower cross-validated RMSE (0.98 vs 1.32) and a higher cross-validated R^2 (0.945 versus 0.901). Next are GBR and ANN (R2 = 0.907 and 0.882). Because RF's piecewise-constant fit is coarse with only 288 training samples, it performed the worst (RMSE = 1.60). The major finding is that all kernel, boosting, and network models recreate dilution to roughly 1 percentage point on a 72-sample test set; discrepancies between the top three models fall within sampling noise.

TABLE III. PERFORMANCE PARAMETER (TEST SET; CV = 5-FOLD)

Model	**MAE**	**RMSE**	**R^2**
linear	0.71	0.92	0.95
SVR	0.77	0.99	0.94
Random Forest	1.23	1.59	0.86
GBR	0.59	0.72	0.97
ANN	1.21	1.54	0.86

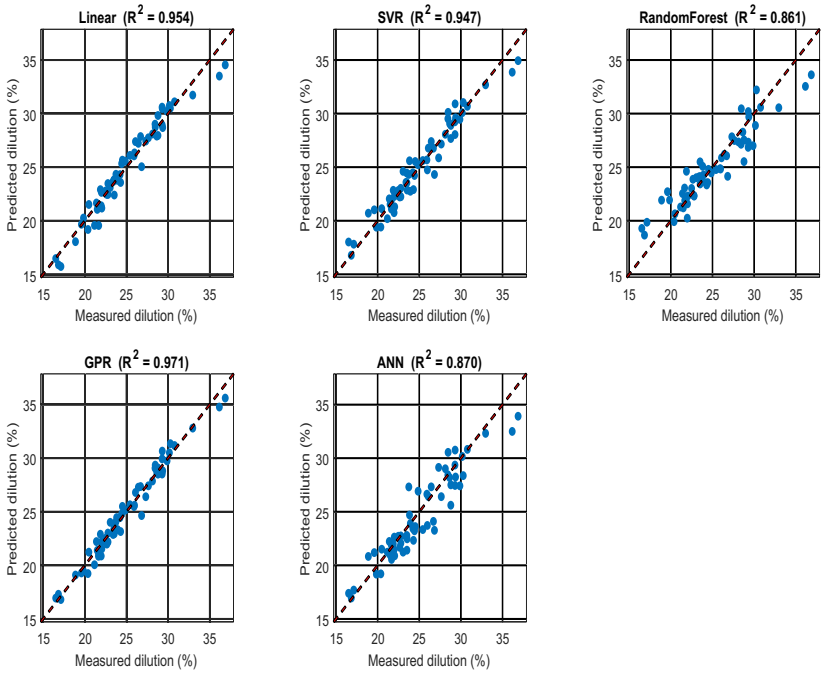

Fig. 4. Predicted versus simulated-measured dilution on the test set for SVR (dashed line: ideal).

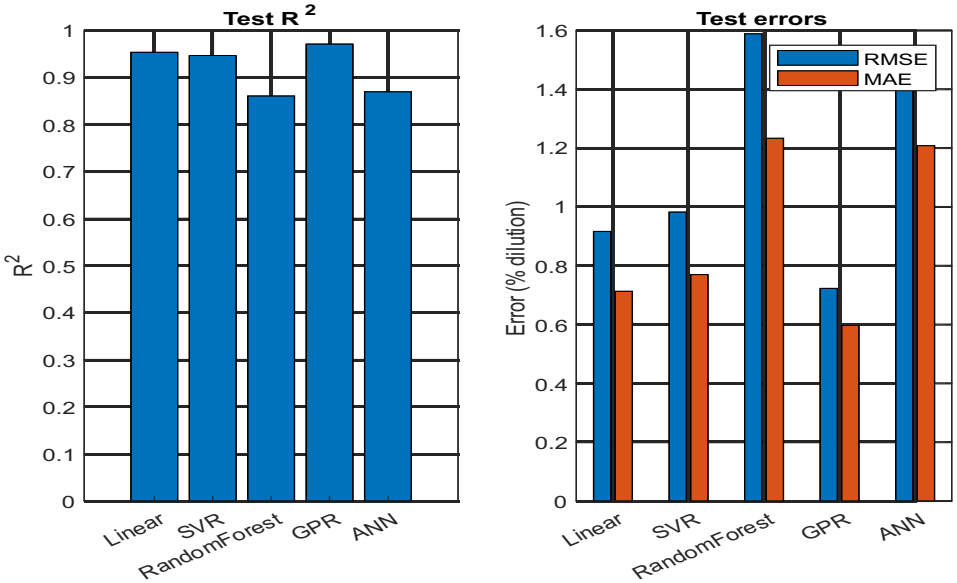

Fig. 5. Test R^2 and Test errors of the five models.

B. Input Influence

With results expressed in percentage points of RMSE increase, permutation importance (Fig. 6) ranks the inputs as I (3.14), v (3.04), WFS (2.70), U (2.54), and CTWD (0.35). As would be expected from Eqs. (1)–(3), where they set HI and A, current, travel speed, wire feed rate, and voltage have similar effects. Since CTWD has little effect in the generating model by design, this ranking reflects the simulator and needs to be re-derived from real data.The expected response surface with U = 24 V, CTWD = 17 mm, and WFS = 0.04I is displayed in Fig. 7. Due to the fact that both HI and the reinforcement area per unit length vary with v, dilution significantly reduces with travel speed. Because the WFS coupling rises A and B simultaneously as current increases, the D = 8% contour falls between roughly 7.5 and 8.2 mm/s across the current range.

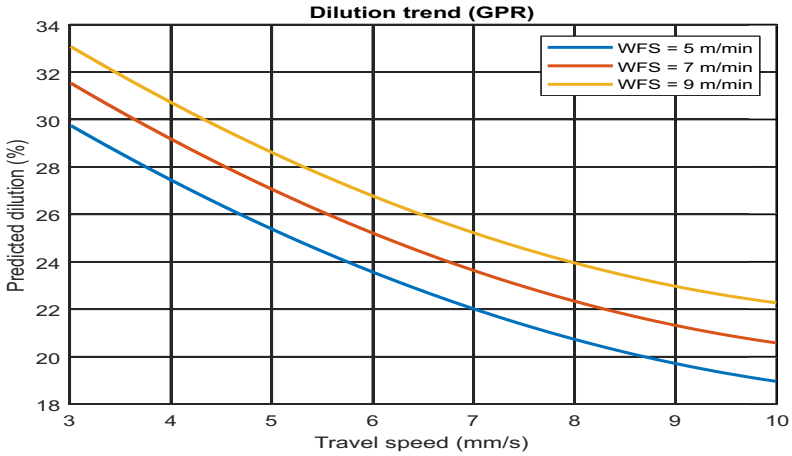

Fig. 6. Variation of prediction speed and travel speed

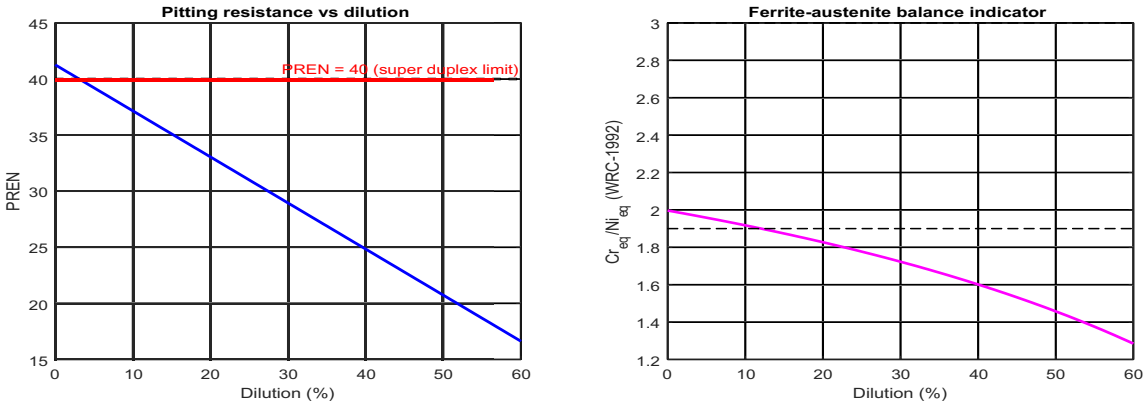

Fig. 7. Predicted dilution (%) versus PREN & Variation of Dilution(%) with WRC

C. Optimised Parameters

Within roughly 35 generations, all five GA runs reached a comparable peak fitness (Fig. 8). The optimal solution (Table IV) has a predicted dilution of 7.34% and WFS = 11.40 m/min. At the same parameters, evaluating the noise-free process model yields 7.20% (HI = 0.70 kJ/mm, A = 34.4 mm² B = 2.67 mm². This is not an experimental confirmation; rather, it is a model-consistency check. The GA solution is 6.0% higher than the highest possible (D ≤ 8%) WFS of the 360 produced samples, which is 10.76 m/min.

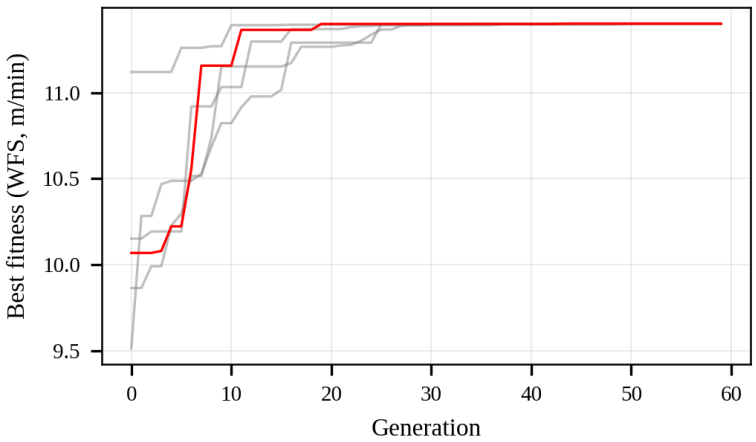

Fig. 8. GA convergence for five independent runs (best run in red).

TABLE IV. OPTIMISED PARAMETER SET

Variable	Optimum	Bounds
Current I (A)	260.0	120–260
Voltage U (V)	21.0	18–30
Travel speed v (mm/s)	6.24	3–10
WFS (m/min)	11.40	4–12
CTWD (mm)	17.7	12–22
Predicted D (%)	7.34	≤ 8

* This result is qualified by two observations. First, the dilution constraint is inactive: the solution lies on the edge of the training area where surrogate extrapolation is least trustworthy since it is constrained by the WFS coupling (WFS − 0.04I = 1.0) and the current upper bound (260 A). Second, Eqs. (5) and (6) yield a first-layer PREN of 38.9 with D = 7.20%, and Eq. (7)

* yields a second-layer PREN of 41.7, which satisfies PREN ≥ 40 for the Table I compositions.

V. CONCLUSION

This study demonstrates a thorough, repeatable machine-learning method for predicting and controlling the dilution of super duplex stainless steel (SDSS) weld claddings put on carbon steel. Dilution is formalized geometrically using the bead cross-section and chemically using a mixing rule that extends to the Creq/Nieq ratio and the pitting resistance equivalent number (PREN). Five regressors—ridge regression, support vector regression, random forest, gradient boosting, and a multilayer perceptron—are trained using five process inputs: current, voltage, travel speed, wire feed rate, and contact-tip-to-work distance. A real-coded evolutionary algorithm is then used to perform inverse optimization, which maximizes wire feed rate within a dilution limit. Instead of coming from lab trials, the dataset (n = 360) was created using a physics-informed bead-formation model with measurement-scale noise. On the held-out set, support vector regression yielded the best overall result (R^2 = 0.930, RMSE = 1.01 percentage points; five-fold cross-validated R^2 = 0.945). The evolutionary approach converged on a parameter set with an expected dilution of 7.3%, in line with the process model (7.2%). The pipeline is data-agnostic and can be utilized directly with measured macrographs and spectrometry data.

REFERENCES

[1] J. C. Lippold and D. J. Kotecki, Welding Metallurgy and Weldability of Stainless Steels. Hoboken, NJ, USA: Wiley, 2005.

[2] R. N. Gunn, Duplex Stainless Steels: Microstructure, Properties and Applications. Cambridge, U.K.: Woodhead, 1997.

[3] I. Alvarez-Armas and S. Degallaix-Moreuil, Eds., Duplex Stainless Steels. London, U.K.: ISTE/Wiley, 2009.

[4] A. J. Sedriks, Corrosion of Stainless Steels, 2nd ed. New York, NY, USA: Wiley, 1996.

[5] D. J. Kotecki and T. A. Siewert, "WRC-1992 constitution diagram for stainless steel weld metals: A modification of the WRC-1988 diagram," Weld. J., vol. 71, no. 5, pp. 171-s–178-s, 1992.

[6] T. Kannan and N. Murugan, "Effect of flux cored arc welding process parameters on duplex stainless steel clad quality," J. Mater. Process. Technol., vol. 176, nos. 1–3, pp. 230–239, 2006.

[7] N. Murugan and R. S. Parmar, "Effects of MIG process parameters on the geometry of the bead in the automatic surfacing of stainless steel," J. Mater. Process. Technol., vol. 41, no. 4, pp. 381–398, 1994.

[8] D. S. Nagesh and G. L. Datta, "Prediction of weld bead geometry and penetration in shielded metal-arc welding using artificial neural networks," J. Mater. Process. Technol., vol. 123, no. 2, pp. 303–312, 2002.

[9] D. E. Rumelhart, G. E. Hinton, and R. J. Williams, "Learning representations by back-propagating errors," Nature, vol. 323, pp. 533–536, 1986.

[10] L. Breiman, "Random forests," Mach. Learn., vol. 45, no. 1, pp. 5–32, 2001.

[11] J. H. Friedman, "Greedy function approximation: A gradient boosting machine," Ann. Statist., vol. 29, no. 5, pp. 1189–1232, 2001.

[12] J. H. Holland, Adaptation in Natural and Artificial Systems. Ann Arbor, MI, USA: Univ. Michigan Press, 1975.

[13] F. Pedregosa et al., "Scikit-learn: Machine learning in Python," J. Mach. Learn. Res., vol. 12, pp. 2825–2830, 2011.

[14] C. Cortes and V. Vapnik, "Support-vector networks," Mach. Learn., vol. 20, no. 3, pp. 273–297, 1995.

[15] J. C. Lippold and D. J. Kotecki, Welding Metallurgy and Weldability of Stainless Steels. Hoboken, NJ, USA: Wiley, 2005.

[16] J. Nilsson, "Super duplex stainless steels," Mater. Sci. Technol., vol. 8, no. 8, pp. 685–700, 1992.
[17] S. Kou, Welding Metallurgy, 2nd ed. Hoboken, NJ, USA: Wiley, 2003.
[18] I. S. Kannan and N. Murugan, "Effect of flux cored arc welding process parameters on duplex stainless steel clad quality," J. Mater. Process. Technol., vol. 176, no. 1–3, pp. 230–239, 2006.
[19] N. Murugan and R. S. Parmar, "Effects of MIG process parameters on the geometry of the bead in the automatic surfacing of stainless steel," J. Mater. Process. Technol., vol. 41, no. 4, pp. 381–398, 1994.
[20] J. Goldak, A. Chakravarti, and M. Bibby, "A new finite element model for welding heat sources," Metall. Trans. B, vol. 15, no. 2, pp. 299–305, 1984.
[21] K. Hornik, M. Stinchcombe, and H. White, "Multilayer feedforward networks are universal approximators," Neural Netw., vol. 2, no. 5, pp. 359–366, 1989.
[22] L. Breiman, "Random forests," Mach. Learn., vol. 45, no. 1, pp. 5–32, 2001.
[23] T. Chen and C. Guestrin, "XGBoost: A scalable tree boosting system," in Proc. 22nd ACM SIGKDD Int. Conf. Knowl. Discovery Data Mining, San Francisco, CA, USA, 2016, pp. 785–794.
[24] R. Storn and K. Price, "Differential evolution—A simple and efficient heuristic for global optimization over continuous spaces," J. Global Optim., vol. 11, no. 4, pp. 341–359, 1997.
[25] K. Deb, A. Pratap, S. Agarwal, and T. Meyarivan, "A fast and elitist multiobjective genetic algorithm: NSGA-II," IEEE Trans. Evol. Comput., vol. 6, no. 2, pp. 182–197, Apr. 2002.